CrystEngComm

RSC Publishing

PAPER

View Article Online
View Journal | View Issue

Cite this: *CrystEngComm*, 2013, **15**, 4507

Nanoscale and microscale structural changes alter the critical gelator concentration of self-assembled fibrillar networks

J. Gao,[a] S. Wu,[a] T. J. Emge[b] and M. A. Rogers*[a]

Received 21st February 2013,
Accepted 22nd April 2013

DOI: 10.1039/c3ce40323h

www.rsc.org/crystengcomm

It has been well established that self-assembled fibrillar networks require a meticulous balance between opposing molecular forces that control solubility and those intermolecular forces that direct epitaxial growth into axially symmetric elongated aggregates. The chemistry of the continuous phase (*i.e.*, solvent) influences every level of structure in molecular gels. Solvent parameters induce low molecular weight gelators (LMOGs) to crystallize into different polymorphic forms, as well cause changes in the lamellar arrangement and domain size. These nanoscale alterations cause measureable differences in the microstructure, which induce physical macroscopic changes including the critical gelator concentration, melting temperature, melting enthalpy and opacity of the gel. Specifically, some solvents cause 12-hydroxyoctadecanoic acid (12HOA) to self-assemble into triclinic parallel polymorphic forms where the lamellar spacing indicates that 12HOA forms an interdigitated network (lamellar spacing <46 Å). The resulting molecular gels are opaque due to the presence of spherulitic crystals and have elevated critical gelator concentrations (*i.e.*, greater than 1.5 wt%). Conversely, other solvents result in the formation hexagonal polymorphs and an extended bi-molecular length greater than 46 Å observed in the lamellar spacing. In these solvents, 12HOA forms translucent molecular gels, at concentrations less than 1.5 wt%, comprised of axially symmetric elongated crystals.

Introduction

Organogels are thermoreversible quasi-solid soft materials consisting of low-molecular weight organogelators (LMOG) in organic liquids (usually $\geqslant 95$ wt%). LMOGs self-assemble *via* physical interactions, including hydrogen-bonding,[1–4] π–π stacking,[5] dipole–dipole interactions,[6,7] and London dispersion forces,[8] into 3-dimensional networks.[9–11] The solvent-gelator specific (*i.e.*, H-bonding) and nonspecific (dipole–dipole, dipole-induced and instantaneous dipole induced forces) intermolecular interactions are equally important in establishing the continuous three-dimensional network.[12,13] Self-assembly, in molecular gels, is an intricate process that must balance solubility and those intermolecular forces that control epitaxial growth into axially symmetric elongated aggregates.[10,13–16] During assembly, individual molecules are driven to aggregate by molecular self-recognition and intermolecular non-covalent interactions into oligomers and subsequently, these oligomers assemble into fibrillar aggregates immobilizing the solvent *via* capillary forces.[17,18]

12HOA, a structurally simple, highly effective LMOG has been studied extensively.[2,3,15,19–32] Critical interactions between the solvent and 12HOA govern the physical behavior and gelation process.[12] Self-assembly begins, in LMOGs, after a critical concentration is achieved, below which the gelator is soluble existing primarily as monomers in solution.[12] After sufficient addition of gelator molecules, the critical concentration is reached and gelation begins, leading to a decrease in the concentration of gelator in the solution phase.[12] Further addition of gelator molecules cause the solvent to be immobilized but that does not alter the soluble concentration of gelator molecules.[12] Since gelator solubility is dependent on the nature of the solvent, most studies stop at correlating critical gelator concentration (CGC) to solubility parameters.[12,13]

Reports by Gao *et al.*,[13] and Yan *et al.*,[33] have both shown that the CGC increases as the polar and hydrogen-bonding Hansen solubility parameters (HSP) increase irrespective of the gelator chemistry. A recent report went beyond the CGC effects and found solvents modify interactions between pyrenyl group interactions in pyrenyl-linker-glucono gelators.[33] In this current work, we use 12-hydroxyoctadecanoic acid to study the nanostructure and microstructure of the gels in different solvents with CCG's varying between 0.2 to 2.5 wt%.

[a]*School of Environmental and Biological Sciences, Department of Food Science, Rutgers University, The State University of New Jersey, New Brunswick, NJ 08901, USA. E-mail: rogers@AESOP.Rutgers.edu*
[b]*School of Arts and Science, Department of Chemistry and Chemical Biology, Rutgers University, The State University of New Jersey, Piscataway, NJ 08854, USA*

Table 1 Critical gelator concentration determined using the inverted vial technique for the studied solvents and the acronym use to identify the points on individual figures

Solvent	Acronym	CCG (wt%)
Hexane	6-ane	0.4
Heptane	7-ane	0.3
Octane	8-ane	0.3
Nonane	9-ane	0.25
Decane	10-ane	0.2
Dodecane	12-ane	0.2
Octanal	8-al	2.5
Nonanal	9-al	2.5
Decanal	10-al	1.6
4-Heptone	7-one	2.4
5-Nonanone	9-one	2.1
6-Undecanone	11-one	1.6
Dipropyl ether	7-eth	2.2
Dibutyl ether	9-eth	1.5
Dipentyl ether	11-eth	1.4
Ethanenitrile	2-nit	2.3
Propanenitrile	3-nit	2.3
Butanenitrile	4-nit	2.1
Octanenitrile	6-nit	1.5
Nonanenitrile	9-nit	0.9
1-Pentanethiol	5-thi	0.5
1-Hexanethiol	6-thi	0.45
1-Heptanethiol	7-thi	0.45
1-Octanethiol	8-thi	0.4
1-Decanethiol	10-thi	0.3

Methods

Solvent selection criteria were maintained as simply as possible with the aliphatic chain being linear, saturated, the functional group located in the primary position and the solvent must be in a liquid state between 10 and 30 °C. The only exceptions to these selection criteria were the ethers and ketones where the functional group was located in the exact middle of the molecule. Apolar solvents included the aliphatics, polar solvents were subdivided into four categories: aldehydes, ketones, ethers and nitriles; as well, the solvents capable of hydrogen bonding were divided into two groups; thiols and amines (Table 1). All solvents and D-12-hydroxyoctadecanoic acid (12HOA) were obtained from Sigma-Aldrich (Cherry Hill, NJ, USA) with purity greater than 0.95%.

Sample preparation and gel test

12HOA was dispersed in 2 ml of solvent in 4 ml glass vials capped with PTFE lined lids (VWR, Randor, PA). 12HOA was studied in numerous solvents (Table 1) and the concentration was studied at 0.1% increments from 0.1 wt% to 3 wt%. After 12HOA was dispersed in each solvent and was capped, the vials were placed in a hot water bath set at 95 °C for 20 min. After the sol appeared clear, it was removed and stored for 24 hours at 20 °C in the chemical fumehood. To determine if the material was a gel, the vial was inverted for 1 hour and if the material did not flow it was considered gelled. This method had to be employed due to the extremely high volatility of several of the solvents employed.

Free induction decay-NMR measurements

Samples of 2 wt% 12HOA in various solvents were subjected to T_2 relaxation measurements on a Bruker mq20 Series NMR Analyzer (Bruker, Milton, Ontario, Canada). A Hahn-echo pulse sequence was used to measure the Free Induction Decay (FID). The operational pulse length was obtained using the calibration procedures recommended by the manufacturer. The 90° pulse was 2.6 μs and the 180° pulse was 5.1 μs. This allowed determination of the gain (64) and recycle delay (5 s). Tau was selected to be as short as possible (0.5 ms) to minimize chemical exchange and diffusion effects on the decay curves.

Differential scanning calorimetry

10 to 12 mg samples of 2 wt% 12HSA in various organic solvents were transferred into Alod-Al hermetic DSC pans. The DSC chamber (Q2000, TA instruments, New Castle, DE) was pre-cooled to 20 °C before the sample was placed into the chamber which was continually flushed with nitrogen (0.5 ml min^{-1}). The samples were heated to 90 °C and cooled to 20 °C at 2 °C min^{-1} to determine the peak crystallization and melting temperatures. The enthalpy of melt was determined by integrating the endothermic transition using the software's tangent skimming method.

Microscopy

The supramolecular structure of 2 wt% 12HOA in various solvents was imaged using a Linkham Imagining station (Linkham, Surrey, England) equipped with a Q imagining 2560 × 1920 pixel CCD camera (Micropublisher, Surrey, Canada) and a 10X Olympus lens (0.25 N.A.) (Olympus, Tokyo, Japan). Samples were placed on a glass slide and a cover slip was placed on top of the sample. The slide was transferred into a Peltier temperature control stage (LTS120, Linkham, Surrey, England) using a water reservoir as the heat sink. The samples were heated to 80 °C and cooled at 2 °C min^{-1} to 20 °C to observe fiber formation using non-polarized light. Light micrographs were calibration with a 100 μm micrometer.

Fourier transform infrared spectroscopy

A small portion of 2 wt% HOA gel was removed directly from the glass vial after 24 hours of storage and was placed directly on the Attenuated total refraction (ATR) prism in a Thermo Nicolet FT-IR (Thermo Fisher Scientific, MA, USA). 256 scans were collected at a resolution of 4 cm^{-1} using an empty cell as the background for the FT-IR measurements. The carbonyl (~1700 cm^{-1}) and hydroxyl (~3200 cm^{-1}) signals were measured.

X-Ray diffraction

2 wt% 12HOA gels were loaded into 0.5 mm silica capillaries and were flame sealed. The capillaries, containing sample, were placed into an Enraf-Nonius FR571 rotating anode X-ray generator equipped with Rigaku Osmic mirror optic system ($\sim$0.06 deg 2q nominal dispersion for Cu Ka; λ = 1.5418 Å) and a Bruker HiStar area detector operating at 40 kV and 40 mA. The X-ray diffraction (XRD) or wide-angle X-ray scattering (WAXS) patterns of 12HOA gels were collected at room temperature over a period of 300 s. The sample to detector distance was 10.0 cm and the standard spatial calibration was performed at that distance. Scans were 4 degrees wide in omega (w) with fixed detector, or Bragg angle (2q) of 0 deg, and fixed platform (f and c) angles of 0 and 45 deg, respectively. In all cases, the count rate for the area detector did not exceed 100 000 cps.

Discussion

The CGC of 12HOA varies between 0.2 wt% and 2.5 wt% depending on the solvent used as the continuous phase (Table 1).[13] The CGC, using the selected solvents, had to be determined using the tube inversion method due to the extreme solvent volatility. However, this technique and similar techniques (''falling ball'' method) have been employed previously to determine the CGC of molecular gels.[13,26,33,34] It is not surprising that modifying the chemistry of the solvent modifies the CGC, as it has previously been reported that solvent parameters influence the supramolecular structure of LMOGs. The presence or absence of solvent gelator interaction may induce changes in the fiber thickness, the number of junction zones between fibers and the sense of helical twist within the fiber.[12,18] These changes have been shown to not only modify the CGC of 12HOA molecular gels but they also alter the opacity.[13] Apart from observing the CGC and the gel opacity few structure-function mechanisms between solvent structure and gelator have been studied.[33]

In the case of 12HOA, the molecular gel is comprise of self-assembled fibrillar networks (SAFiN) driven to assemble by enthalpic forces forming a network of crystalline fibers.[10] The crystalline nature of the fibers has resulted in numerous research groups developing and applying crystallographic mismatch theory to molecular gels.[2,24,35–37] Structural features that effect crystal perfection include: crystallographic mismatches, solvent inclusions, different polymorphic forms and high crystal surface area to volume ratios. The ''degree of crystallinity'' can be probed using the T_2 relaxation and amplitude obtained using a free induction decay (FID) pulse sequence coupled with pulsed nuclear magnetic resonance (pNMR) (Fig. 1A and B) or using the onset of the melting (Fig. 2B and C) and enthalpy of the transition (Fig. 2D and E) determined using DSC.

T_2 relaxations, below 70 μs, are proportional to the perfection of the crystalline phase.[30,31] A high degree of 'crystallinity' is correlated to shorter T_2 free induction times[38]

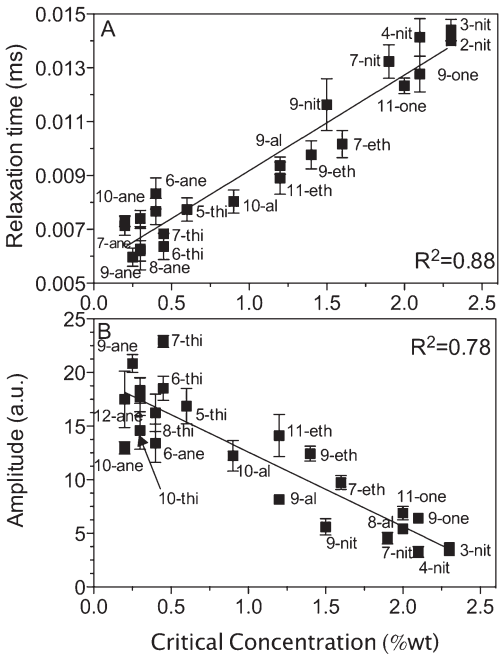

Fig. 1 Pulse NMR proton free induction decay relaxation times (A), decay amplitudes (B) for 2 wt% 12-hydroxyoctadecanoic acid molecular gels in various organic solvents.

and relates to numerous structural features of crystals suspended in solvents. For 12HOA, a positive linear correlation was found between the T_2 relaxation time and the CGC (Fig. 1A). Although this suggests that as the CGC increases there is a decrease in the crystal perfection; the nature of the crystal imperfections cannot be elucidated using this technique. For example, the decrease in crystal perfection may be related to several structural changes such as: different polymorphic forms, the number of solvent inclusions, the amount of interfacial area between the 12HSA and solvent, or any combination thereof.

The T_2 decay amplitude, obtained from the FID provides additional useful information regarding the crystalline nature of the SAFiNs (Fig. 1B). A negative correlation between the T_2 amplitude CGC is observed (Fig. 1B). This suggests that as the CGC increases, the solubility of the gelator also increases resulting in less crystalline mass. As the solvent conditions change (*i.e.*, increasing polar and hydrogen bonding Hansen solubility parameters), the CGC increase to a point, after which 12HOA becomes soluble in the solvent and corresponds to a T_2 FID decay amplitude at or near zero.

The onset of the melting temperature (Fig. 2B and C) is also related to the degree of crystalline order. In polymer systems, a decrease in T_m is observed upon the addition of a solvent, which acts as a plasticizer.[39] A decrease in the melting temperature is associated with an increase in the surface area associated with the crystalline phase of the molecular gel; therefore, changes in the melting temperature may be explained using Gibbs free-energy curves.[23] For 12HOA, the CGC was negatively correlated with the crystallization and

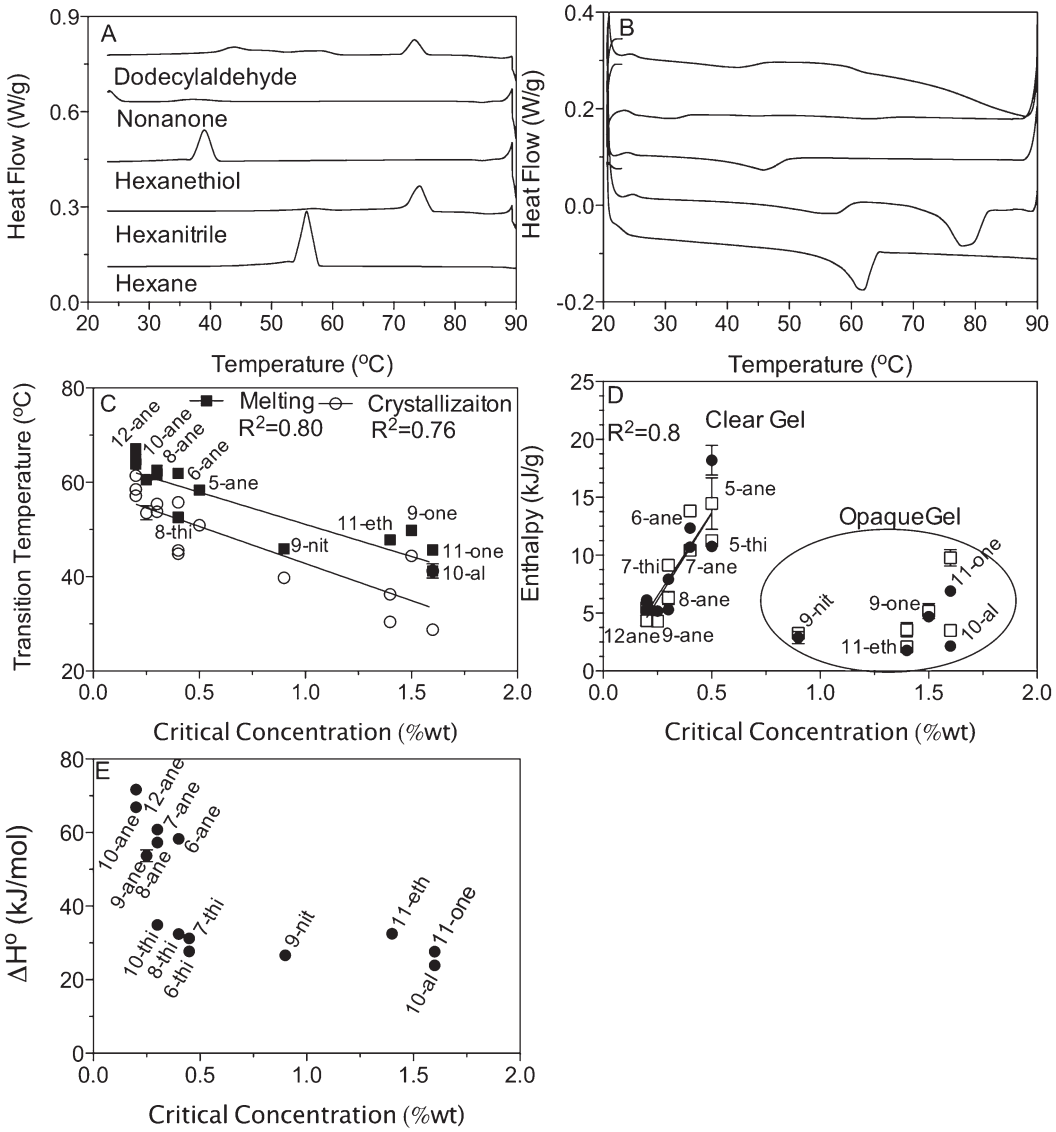

Fig. 2 DSC thermograms of the exothermic crystallization (A) and endothermic melting transition (B) of 12HOA molecule gels. Crystallization and melting temperatures (C) and melting enthalpies obtained by integration of the thermograms (D) and the Hildebrand solubility equation (E) for 12HOA molecular gels in several organic solvents.

melting temperature (Fig. 2C). This signifies that an increase in the CGC corresponds to a decrease in the crystal size and/or more imperfect crystals are present.[39] Comparing the onset of melt (Fig. 2A and C) and the relaxation time (Fig. 1A) both indicate a decrease in the 'crystallinity' with increasing CGC.

The enthalpy of the transition may be attained by integrating the DSC thermograms (Fig. 2D) as well as by using the Hidebrand solubility parameter (Fig. 2E), which is derived from Van't Hoff equation using the onset temperature of melting:[40]

$$\log_{10} x = \frac{\Delta H}{R}\left(\frac{1}{T_m} - \frac{1}{T}\right)$$

where x represents the mol fraction of the higher melting component, ΔH is the enthalpy of melt for the higher melting component, R is the universal gas constant, and T_m and T are the melting temperatures of the higher melting fraction and the gel, respectively. The enthalpy of melt, determined by integrating the DSC thermograms, increased as a CGC increases and then drastically decreases once the CGC reached ~1.0 wt% (Fig. 2D). The increase in the enthalpy, below 1 wt%, contradicts observations made using pNMR, which suggest that the amount of crystalline materials decreases as CGC increases (Fig. 1B). This contradiction, along with previous observations that the gels undergo a transition from a translucent to an opaque gel at CGCs at ~1 wt%,[13] were used to formulate the hypothesis that the molecular arrangement of 12HOA differs in dissimilar solvents giving rise to different intermolecular non-covalent interactions causing a drastic modification in the macroscopic properties of the gel. Hence, the amount of energy released during the phase

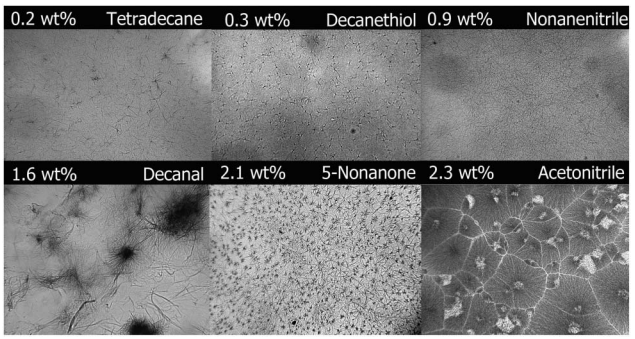

Fig. 3 Light micrographs of 2 wt% 12-hydroxyoctadecanoic acid organogels in different organic solvents. Critical gelator concentration of 12-HSA in each solvent is displayed in upper left corner. Width of micrograph is 120 μm.

transition is a function of both the amount of crystalline mass and also the nature of the non-covalent interactions between 12HOA molecules.

In order to more accurately probe the solubility issues of the 12HOA gels the enthalpy was calculated using the Hildebrand solubility equation. Using this method, the enthalpy is determined based on the chemical equilibrium at a specific temperature. This suggests that the enthalpy will be solely a measure of the amount of crystalline 12HOA molecules. The enthalpy of melt, determined using the Hildebrand solubility equation was negatively correlated with the CGC (Fig. 2E) corresponding to the observations made using the T_2 relaxation amplitude (Fig. 1B).

The difference between 12HOA gels in different solvents measured using pNMR and DSC, along with previous observations in the visual opacity compelled the examination of microstructure and nanostructure. To probe the microstructure of 12HOA gels brightfield microscopy was employed (Fig. 3). CGC, less than 1 wt%, assembled into axially symmetric elongated aggregates radiating from central nuclei. These fibers are only a few microns in width but may exceed 100 μm in length (Fig. 3, top row). The lack of junction zones and narrow fiber width cause them to appear transparent because the structural units an incapable of diffracting light. At low CGCs thin fibers are observed; however, as the CGC increases there is a transition to dense clusters of fibers and eventually to spherulitic structures. The transition from fibril aggregates to spherulitic crystals, in molecular gels, arises due to crystallographic mismatches.[35,36] These crystal imperfections which lead to the generation of spherulitic crystals coincides with the reduced 'crystallinity' observed using pNMR and DSC which confirms in part that the molecular arrangement of 12HOA differs in dissimilar solvents giving rise to different intermolecular non-covalent interactions.

The changes in the supramolecular structure provide some clarification to the decrease in the crystalline order measured using the relaxation time and amplitude (Fig. 1A), and the enthalpy of melt and onset of melt (Fig. 2). However, as the CGC increases, the major changes to the supramolecular 12HSA network structure must be driven either due to a co-

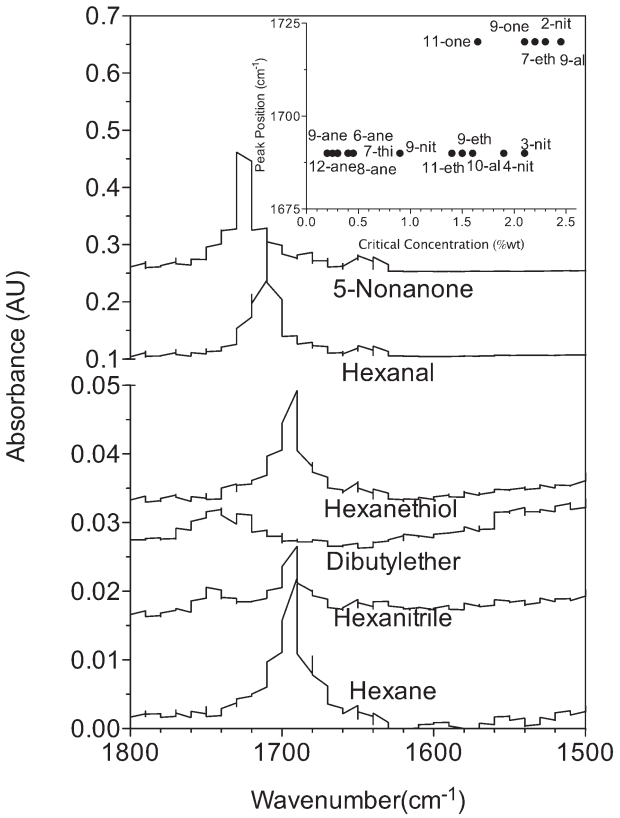

Fig. 4 Vertically offset FT-IR spectra focusing on the carboxylic acid region of 12HSA molecular gels in various solvents using the air as the background. (Inset: FT-IR carboxylic acid peak position of 2.5 wt% 12HSA molecular gels in various solvents as a function of CGC.)

crystallization of the gelator and solvent or different molecular packings within the crystal occur. The non-covalent interactions between 12HOA molecules (Fig. 4) and the molecular arrangements (Fig. 5) were studied using FT-IR and XRD.

Using FT-IR, 12HOA has been shown to form carboxylic acid dimers and the longitudinal growth is driven by interactions between the 12 hydroxyl groups between adjacent molecules.[1,41] Cyclic dimers have a peak position at 1690 cm^{-1} while free monomers appear at 1720 cm^{-1} (Fig. 4). When the critical concentration is less than 1.5 wt%, 12HOA is able to form dimers and Above 1.5 wt%, depending on the solvent; 12HOA can either exist as monomers or dimers (Fig. 4, insert). The existence of 12HSA monomers corresponds to a lower enthalpy of melt and crystallization due impart to fewer physical bonds in the network structure (Fig. 2).

Structural changes were also probed using XRD (Fig. 5). In general, the 001 and higher order 003 peaks could be resolved (Fig. 5A). However, no obvious changes were observed with the exception of the aldehydes, which had a very broad 001 peak. The wide-angle spacings showed much more deviation between samples (Fig. 5B). Some solvents exhibited a hexagonal sub cell spacing (~4.3 Å) while others showed a triclinic parallel sub cell (strong peak at 4.6 Å, and two weak peaks at 3.9 Å and 3.8 Å) (Fig. 5B) which has been previously

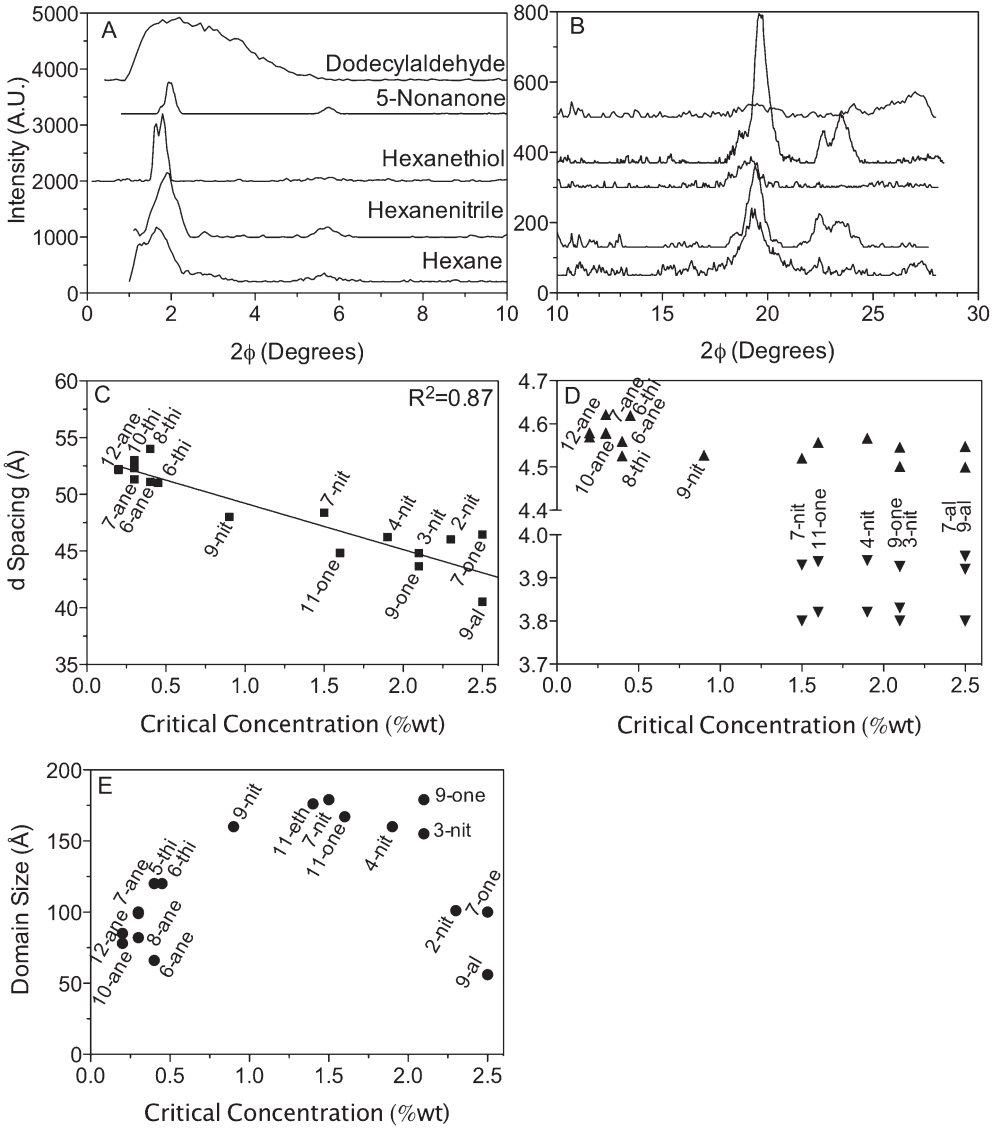

Fig. 5 Vertically offset wide-angle (A) and short-angle (B) diffractograms for 12HOA in various solvents. The long (C) and short spacings (D) obtained from XRD and the domain size (E) calculated using the Williamson Hull equation for 12HOA molecular gels as a function of CGC.

shown.[42] The *d* spacing of the 001 wide-angle spacing was plotted as a function of CGC and an inverse correlation was observed (Fig. 5C). At low CGCs the *d*-spacing was slightly longer than the bimolecular length of 12HOA, while at CGCs greater than ~1.5 wt% the *d*-spacing was shorter than the bimolecular length of 12HOA. This supports the observation that when cyclic dimers form, the *d*-spacing must exceed the extended bimolecular length. However, if 12HSA does not effectively form a dimer than the *d*-spacing may be less than the bimolecular length suggesting interdigitation of 12HSA in the crystals. Along with the change to the carboxylic head group and the bimolecular length, a polymorphic transition was also observed. Low CGCs correspond to a hexagonal sub cell spacing and above 1.5 wt% the triclinic parallel sub cell spacing is observed (Fig. 5D).

The full width half max for each peak was obtained and using a Williamson Hull equation the domain size was obtained. The Williamson Hull equation is:[43]

$$\mathrm{FW}(S)x\cos(\theta) = \frac{K\lambda}{\mathrm{size}} + (4(\mathrm{strain})\sin(\theta))$$

where FW is the full-width half-max, θ is the diffraction angle, K is the Scherrer constant, λ is the *x* ray wavelength. The Williamson Hull plots FW(S)*x*cos(θ) *versus* sin(θ). Since few diffraction peaks were observed we had to assume that there was no strain and hence the slope was set equal to zero. From the *y*-intercept, the domain size was calculated and plotted against the CGC (Fig. 5E). The domain size follows a parabolic shape when plotted against the CGC. The vertex of the parabola corresponds to a transition from the hexagonal sub cell to the triclinic parallel sub cell. As the CGC increases from 0.2 to 1.5 wt% (corresponding with an

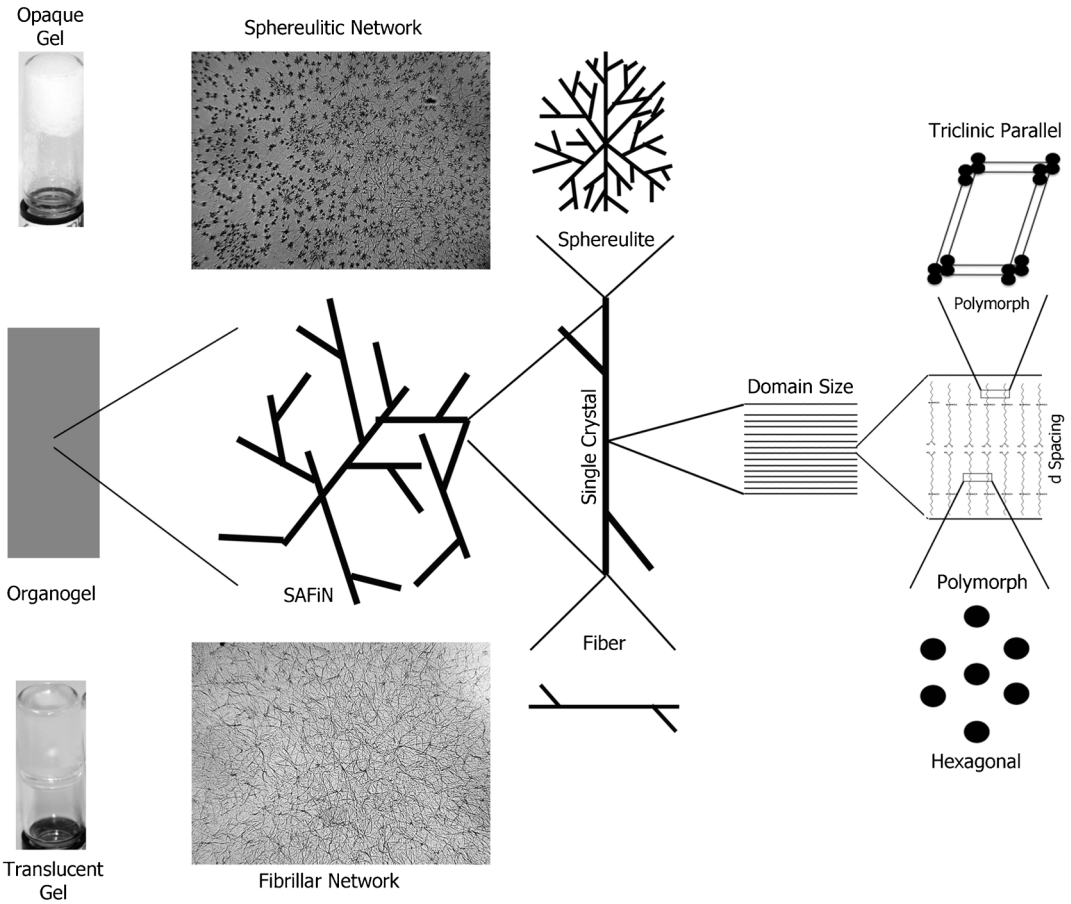

Fig. 6 Different levels of structure examined in this structure which are effected by the solvent properties and CGC.

increase in the δ_p and δ_h) the solvent properties causes an increase in the domain size. At CGCs greater than 1.5 wt%, the domain size decreases as the CGC increases.

What is astonishing about this study is solvent not only effects final physical properties and macroscopic appearance of the gel but also the microscopic structure and nanostructure (Fig. 6). In molecular gels, the solvent structure is as important as the gelator structure when trying to understand how and why certain compounds are capable of self-assembling into axially symmetric elongated aggregates capable of entraining hundreds if not thousands of solvent molecules per gelator molecule.

Conclusions

Modifying the solvent in molecular gels effects the CGC, physical properties of the gels and the opacity. The CGC changes because of changes in the gelator solubility, altered polymorphic crystal forms, and microscopic changes in the network structure. For 12HOA, solvents that require concentrations greater than 1.5 wt% to form molecular gels have spherulitic crystals, a triclinic parallel polymorphic form and the 12HOA molecules are interdigitated. Conversely, translucence gels at concentrations less than 1.5 wt% result from the formation of a fibrillar crystal network, with a hexagonal polymorph and the *d* spacing is greater than the bimolecular length.

References

1 T. Kuwahara, et al., Crystal structure of DL-12-hydroxystearic acid, *Chem. Lett.*, 1996, **25**, 435–436.
2 R. Lam, et al., A molecular insight into the nature of crystallographic mismatches in self-assembled fibrillar networks under non-isothermal crystallization conditions, *Soft Matter*, 2010, **6**(2), 404–408.
3 J. L. Li, et al., Arichitecture of a biocompatible supramolecular material by supersaturation-driven fabrication of its network, *J. Phys. Chem. B*, 2005, **109**, 24231–24235.
4 M. A. Rogers, et al., Multicomponent hollow tubules formeed using phytosterol and γ-oryzanol-based compounds: an understanding of their molecular embrace, *J. Phys. Chem.*, 2010, **114**, 8278–8295.
5 J. R. Moffat and D. K. Smith, Controlled self-sorting in the assembly of 'multi-gelator' gels, *Chem. Commun.*, 2009, 316–318.
6 T. Brotin, J. P. Devergne and F. Fages, Photostationary fluorescence emission and time resoved spectroscopy of

symmetrically disubstituted anthracenes on the meso and side rings: the unusual behavior of the 1,4 derivative, *Photochem. Photobiol.*, 1992, **55**, 349–358.
7 P. Terech, I. Furman and R. G. Weiss, Structures of organogels based upon cholesteryl 4-(2-anthryloxy)butanoate, a highly efficient luminescing gelator – neutron and X-ray small-angle scattering investigations, *J. Phys. Chem.*, 1995, **99**(23), 9558–9566.
8 J. F. Toro-Vazquez, et al., Relationship between molecular structure and thermo-mechanical properties of candelilla wax and amides derived from (*R*)-12-hydroxystearic acid as gelators of safflower oil, *J. Food Sci.*, 2010, **5**(3), 193–202.
9 V. A. Mallia, et al., Reversible phase transitions within self-assembled fibrillar networks of (*R*)-18-(n-alkylamino)octadecan-7-ols in their carbon tetrachloride gels, *J. Am. Chem. Soc.*, 2011, **133**, 15045–15054.
10 R. G. Weiss and P. Terech, Introduction, in *Molecular Gels: Materials with Self-Assembled Fibrillar Networks*, ed. R. G. Weiss and P. Terech, Springer, Dordrecht, The Neatherlands, 2006, pp. 1–13.
11 M. George and R. G. Weiss, Molecular organogels. Soft matter comprised of low-molecular-mass organic gelators and organic liquids, *Acc. Chem. Res.*, 2006, **39**, 489–497.
12 G. Zhu and J. S. Dordick, Solvent effect on organogel formation by low molecular weight molecules, *Chem. Mater.*, 2006, **18**, 5988–5995.
13 J. Gao, S. Wu and M. A. Rogers, Harnessing Hansen solubility parameters to predict organogel formation, *J. Mater. Chem.*, 2012, **22**, 12651–12658.
14 M. Suzuki, et al., Effects of hydrogen bonding and van der Waals interactions on organogelation using designed low-molecular-weight gelators and gel formation at room temperature, *Langmuir*, 2003, **19**(21), 8622–8624.
15 M. A. Rogers and A. G. Marangoni, Solvent-modulated nucleation and crystallization kinetics of 12-hydroxystearic acid: a nonisothermal approach, *Langmuir*, 2009, **25**(15), 8556–8566.
16 M. Raynal and L. Bouteiller, Organogel formation rationalized by Hansen solubility parameters, *Chem. Commun.*, 2011, **47**, 8271–8273.
17 J. G. Hardy, A. R. Hirst and D. K. Smith, Exploring molecular recognition pathways in one- and two-component gels formed by dendritic lysine-based gelators, *Soft Matter*, 2012, **8**, 3399–3406.
18 W. Edwards, C. A. Lagadec and D. K. Smith, Solvent–gelator interactions – using empirical solvent parameters to better understand the self-assembly of gel-phase materials, *Soft Matter*, 2011, **7**, 110–117.
19 P. Terech, Kinetics of aggregation in a steroid derivative/cyclohexane gelifying system, *J. Colloid Interface Sci.*, 1985, **107**(1), 244–255.
20 M. A. Rogers and A. G. Marangoni, Non-isothermal nucleation and crystallization of 12-hydroxystearic acid in vegetable oils, *Cryst. Growth Des.*, 2008, **8**(12), 4596–4601.
21 R. S. H. Lam and M. A. Rogers, Experimental validation of the modified Avrami model for non-isothermal crystallization conditions, *CrystEngComm*, 2010, **13**, 866–875.
22 J. L. Li, et al., Nanoengineering of a biocompatible organogel by thermal processing, *J. Phys. Chem. B*, 2009, **113**(15), 5011–5015.
23 M. A. Rogers, A. J. Wright and A. G. Marangoni, Engineering the oil binding capacity and crystallinity of self-assembled fibrillar networks of 12-hydroxystearicacid in edible oils, *Soft Matter*, 2008, **4**(7), 1483–1490.
24 R. Y. Wang, et al., Architecture of fiber network: from understanding to engineering of molecular gels, *J. Phys. Chem. B*, 2006, **10**, 25797–25802.
25 F. M. Menger, et al., Chain-substituted lipids in monomolecular films. Effect of polar substituents on molecular packing, *Langmuir*, 1989, **5**, 833–838.
26 V. A. Mallia, et al., Robust organogels from nitrogen-containing derivatives of (*R*)-12-hydroxystearic acid as gelators: comparisons with gels from stearic acid derivatives, *Langmuir*, 2009, **25**(15), 8615–8625.
27 A. L. Fameau, et al., 12-Hydroxystearic acid lipid tubes under various experimental conditions, *J. Colloid Interface Sci.*, 2010, **341**(1), 38–47.
28 D. A. S. Grahame, et al., Influence of chirality on the modes of self-assembly of 12-hydroxystearic acid in molecular gels of mineral oil, *Soft Matter*, 2011, **7**, 7359–7365.
29 X. Huang and R. G. Weiss, Molecular organogels of the sodium salt of (*R*)-12-hydroxystearic acid and their templated syntheses of inorganic oxides, *Tetrahedron*, 2007, **63**(31), 7375–7385.
30 T. Sakurai, et al., A comparative study on chiral and racemic 12-hydroxyoctadecanoic acids in the slutions and aggregation states: does the racemic form really form a gel?, *Bull. Chem. Soc. Jpn.*, 2010, **83**(2), 145–149.
31 P. Terech, et al., Organogels and areogels of racemic and chiral 12-hydroxyoctadecanoic acid, *Langmuir*, 1994, **10**(10), 3406–3418.
32 A. J. Wright and A. G. Marangoni, Time, temperature, and concentration dependence of ricinelaidic acid–canola oil organogelation, *J. Am. Oil Chem. Soc.*, 2007, **84**(1), 3–9.
33 N. Yan, et al., Pyrenyl-linker-glucono gelators. Correlations of gel properties with gelator structures and characterization of solvent effects, *Langmuir*, 2013, **29**, 793–805.
34 Y. Wu, et al., Solvent effects on structure, photoresponse and speed of gelation of a dicholesterol-linked azobenzene organogel, *Soft Matter*, 2011, **7**, 9177–9183.
35 X. Y. Liu and P. D. Sawant, Determination of the fractal characteristic of nanofiber-network formation in supramolecular materials, *ChemPhysChem*, 2002, **4**, 374–377.
36 X. Y. Liu and P. D. Sawant, Mechanism of the formation of self-organized microstructures in soft functional materials, *Adv. Mater.*, 2002, **14**, 421–426.
37 R.-Y. Wang, et al., From kinetic-structure analysis to engineering crystalline fiber networks in soft materials, *Phys. Chem. Chem. Phys.*, 2013, **15**, 3313–3319.
38 F. P. Duval, J. P. M. van Duynhoven and A. Bot, Practical implications of the phasecompositional assessment of lipid-based food products by time-domain NMR, *J. Am. Oil Chem. Soc.*, 2006, **83**, 905–912.
39 D. Farbi, J. Guan and A. Cesaro, Crystallisation and melting behaviour of poly (3-hydroxybutyrate) in dilute solution: towards an understanding of physical gels, *Thermochim. Acta*, 1998, **321**, 3–16.
40 L. H. Wesdorp, et al., Phase Equilibria in Fat, in *Fat Crystal Networks*, ed. A. G. Marangoni, Marcel Dekker, New York, USA, 2005.

41 D. Lin-Vien, et al., *The Handbook of Infrared and Raman Characteristic Frequencies of Organic Molecules*, Academic Press, London, UK, 1991.
42 S. Wu, et al., Solvent induced polymorphic nanoscale transitions for 12-hydroxyoctadecanoic acid molecular gels, *Cryst. Growth Des.*, 2013, **13**, 1360–1366.
43 D. Lou and N. Audebrand, Profile Fitting and Diffraction Line-Broadening Analysis, *Advances in X-ray Diffraction*, 1997, vol. 41, pp. 556–565.